REVISION 3

18th December 2018

A Cationic Rectifier Based on a Graphene Oxide Covered Microhole: Theory and Experiment

Budi Riza Putra [1,2], Koichi Jeremiah Aoki [3], Jingyuan Chen [3], Frank Marken*[1]

[1] *Department of Chemistry, University of Bath, Claverton Down, Bath BA2 7AY, UK*
[2] *Department of Chemistry, Faculty of Mathematics and Natural Sciences, Bogor Agricultural University, Bogor, West Java, Indonesia*
[3] *Department of Applied Physics, University of Fukui, 3-9-1, Bunkyo, Fukui-shi 910-8507, Japan*

To be submitted to Langmuir

Proofs to F. Marken (F.Marken@Bath.ac.uk)

Abstract

Cation transport through nano-channels in graphene oxide can be rectified to give ionic diode devices for future applications for example in desalination. A film of graphene oxide is applied to a 6 μm thick poly-ethylene-terephthalate (PET) substrate with 20 μm diameter microhole and immersed in aqueous HCl solution. Strong diode effects are observed even at high ionic strength (0.5 M). Switching between open and closed states, microhole size effects, and time dependent phenomena are explained based on a simplified theoretical model focusing on the field-driven transport within the microhole region. In aqueous NaCl, competition between Na^+ transport and field-driven heterolytic water splitting are observed, but shown to be significant only at low ionic strength. Therefore, nanostructured graphene oxide is demonstrated to exhibit close to ideal behavior for future application in ionic diode desalination of seawater.

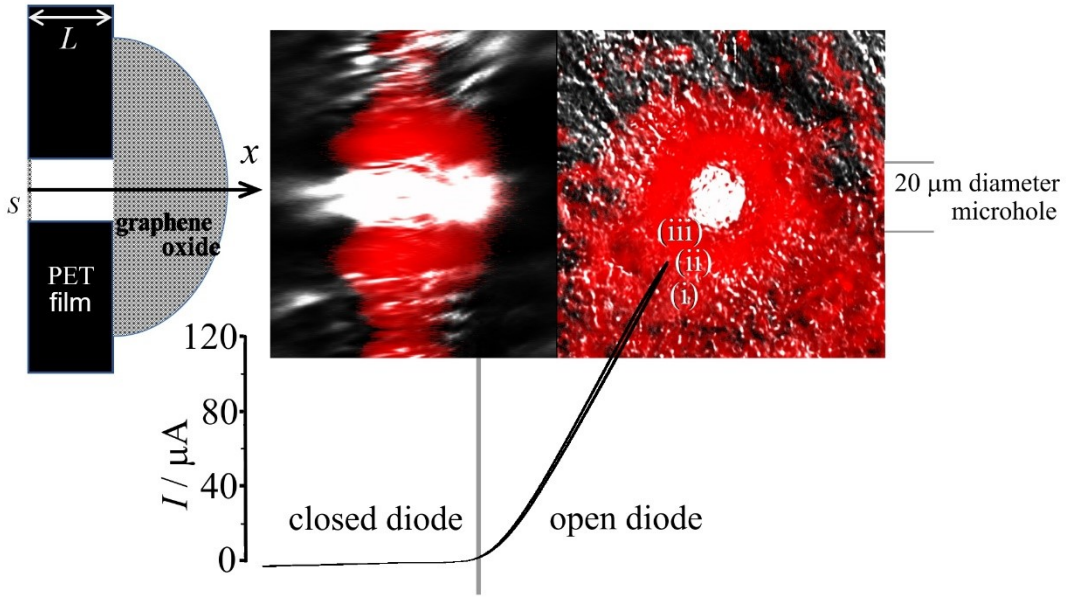

Graphical Abstract

Keywords: desalination, voltammetry, amplifier, transistor, iontronics, molecular pump

1. Introduction

Graphene oxide based materials emerged recently as highly interesting class of nano-material (a sub-class of 2D nano-materials) with some very unusual and potentially beneficial properties.[1] Both graphene derivatives[2,3,4] and graphene oxide[5] materials have been proposed as size selective and tunable water purification membrane components. Graphene oxide materials formed into layered membranes offer selectivity in salt separation and transport.[6] A particular ability has been noted to enhance both water transport[7,8] and small molecule transport.[9,10] Potential for heavy metal removal has been highlighted.[11] The stability or structural integrity of graphene oxide materials in contact to aqueous electrolyte media has been discussed[12] and new composite structures have been suggested for applications that require more robust graphene oxide based membranes.[13,14]

Structural features of graphene oxides (see Figure 1B) result in the possibility of interaction of cations with π-electrons of the graphene oxide layer. This type of interaction is predicted to affect the transport of cations through nanopores within graphene oxide.[15] The importance of graphene oxide in salt separation has been reviewed.[16] Electrically insulating but ionically conducting free-standing membranes produced from graphene oxide materials are of wider interest, for example in energy storage and conversion devices.[17] Fabrication of graphene oxide membranes is commonly based on filter-cake assemblies,[18] but also layer-by-layer assembly,[19] chemical assembly,[20] electrospun membranes,[21] and polymer-blended composites have been reported.[22]

Previous electrochemical studies of ion transport through graphene oxide membranes and composites suggest a relatively high proton conductivity.[23,24] Cation semi-permeability of graphene oxide has been investigated in organic solvent media.[25] The peculiar properties of the graphene oxide nanosheet structure have been suggested to

be linked to the presence of nanochannels and different types of structural regions: (i) regions of pristine graphene causing strong inter-nanosheet interactions, (ii) regions of oxidized graphene allowing proton and water transport, and (iii) holes and defects helping to make the transport more effective. A review has appeared summarizing many of the known membrane transport phenomena in graphene oxide.[26] Analytical applications for ion detection in graphene oxide films have been suggested.[27]

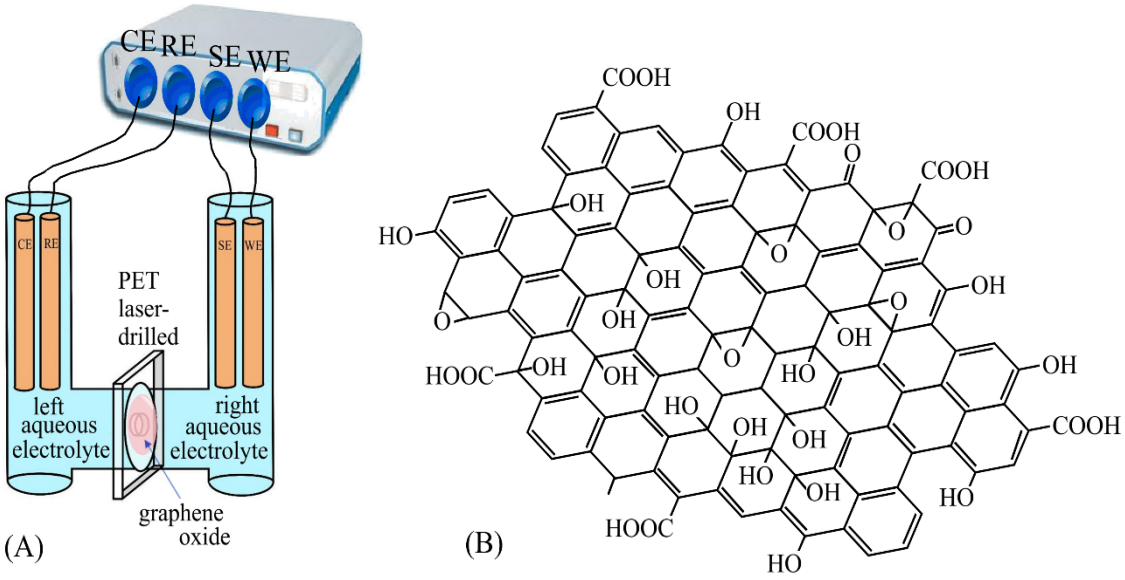

Figure 1. (A) Schematic description of the classic 4-electrode cell for membrane voltammetry (counter electrode CE, reference electrode RE, sense electrode SE, working electrode WE) with graphene oxide deposits on a 6 μm thick PET film with 20 μm diameter microhole. (B) Schematic drawing of a hypothetical graphene oxide structure with hydrophilic regions and hydrophobic regions.

The majority of published work focuses on filtration and ion retention effects for desalination rather than potential driven processes. Furthermore, it was noted that current flow (associated with H_3O^+ or OH^-) was strongly linked to water co-transport

in particular at lower salt concentrations.[28] Therefore, graphene oxide could potentially function as a "molecular pump" for water, if the potential driven ion transport associated with the water transport could be made uni-directional or "diode-like". Diode-like behaviour has been reported for graphene oxide materials interfaced with graphene and coated with electrolyte[29] and a review of ionic rectification mechanisms in membranes has appeared.[30] Ion transport through graphene oxide | ionomer interfaces has been shown to exhibit charge density-controlled rectification.[31] Also, photo-switchable graphene oxide membrane based ionic diodes have been demonstrated by Jiang and coworkers.[32] Here, it is shown here that graphene oxide as a semi-permeable material, when deposited asymmetrically onto a microhole in poly-ethyleneterephthalate (PET), does also lead to diode-like behavior.

In previous work, diode-like behavior was observed for several ion-conducting materials[33,34] as well as for nano-pore systems[35,36,37,38] and for other types of electrolytic systems with structural/compositional asymmetry.[39,40,41] In a previous report, the underlying mechanism for the current rectification or the ionic diode effect for devices based on Nafion ionomer deposited onto a PET microhole has been suggested to be linked mainly to a combination of diffusion-migration and concentration polarization in the microhole region.[42] However, there are a number of different mechanisms to achieve ionic current rectification depending on device scale and composition. Most ionic current rectification phenomena reported more recently are linked to processes at the nanoscale and linked to surface charges.[43] However, also rectification effects in ionomer filled microfluidic channels have been reported[40] and at interfaces between two ionomer materials.[39] Recently, micrometer sized pipettes have been shown to give substantial ionic diode effects, even when a thin polymer brush layer was attached only to the pipet surface.[44] In this report, we describe ionic current rectification effects for the related case of graphene oxide applied to a typically 20 μm diameter hole in PET.

In this exploratory study, we investigate the behavior of graphene oxide deposits on a microhole (20 μm diameter in a 6 μm thick poly-ethylene-terephthalate or PET) in terms of ionic transport under potential polarization conditions. Initially, it is assumed that the ion transport in the presence of aqueous HCl is dominated by proton transport. Later the behavior in other types of aqueous electrolyte media is compared. The experimental lay-out in this study (see Figure 1A) is consistent with that used recently for the study of "ionic diode" phenomena for example for Nafion,[45] cellulose,[46] and polymers of intrinsic microporosity.[47] A conventional two-compartment four-electrode configuration allows the potential applied to the membrane to be monitored and current measured.

As an initial hypothesis it is assumed here that the diode effect is dominated by the diffusion-migration conditions within the asymmetrically graphene oxide coated microhole in the PET film (see Figure 1A). This process relies on graphene oxide acting as a very good semi-permeable cation conductor material with good anion rejection even at high ionic strength. A simplified theoretical model based on analytical theory is suggested to rationalise the appearance of cyclic voltammograms and current rectification effects. Rectification effects are investigated for different electrolyte media and shown to be dominated by cation transport in semi-permeable graphene oxide even under conditions of relatively high ionic strength in the electrolyte. Competing water heterolysis to protons and hydroxide (as a competing process to ion insertion and transfer via graphene oxide) is shown to occur at a significant level only under conditions of low ionic strength. Finally, the concept of ionic diode desalination based on graphene oxide materials as key components in cationic and anionic diodes is proposed.

2. Experimental

2.1. Chemical Reagents

Graphene oxide (2 mg/mL, dispersion in H_2O, Aldrich 763705), concentrated hydrochloric acid (37%), agarose, and rhodamine B (97%) were obtained from Sigma-Aldrich Ltd. and used without further purification. Solutions were prepared under ambient conditions in volumetric flasks with ultrapure water resistivity of 18.2 MΩ cm from an ELGA Purelab Classic System for water filtration.

2.2. Instrumentation

Transmission electron microscopy (TEM) was performed with a JEOL JEM-2100 Plus instrument with 200 kV maximum operating voltage. The fluorescence microcopy instrument was a Zeiss LSM 880 with airyscan and multiphoton laser. Electrochemical data (for voltammetry, chronoamperometry, and impedance experiments) were recorded at T = 20 ± 2 ^{o}C on a potentiostat system (Ivium Compactstat, Netherland). A classic 4-electrode electrochemical cell configuration was employed. The membrane separates two tubular half-cells (15 mm diameter, see Figure 1), one with Pt wire working and KCl-saturated calomel (SCE) sense electrode (right in Figure 1A) and the other with SCE reference electrode and Pt wire counter electrode (left in Figure 1A). In electrochemical measurements, the working electrode was always located on the side of the graphene oxide film deposit. In some measurements, additional battery powered pH-probes (Voltcraft PH-100ATC) were positioned in left and right compartment close to the membrane.

2.3. Graphene Oxide Deposition

The polyethylene-terephthalate (PET) films of 6 μm thickness with laser-drilled 20 μm diameter microhole were obtained from Laser-Micro-Machining Ltd., Birmingham, UK. A microscopy glass slide was pre-coated with a thin layer of 1% agarose gel. The PET film was placed onto the gel to stop liquid entering the microhole (and to define

the interface within the microhole). A 4 μL volume of graphene oxide solution (2 mg/mL in water) was applied to the surface and with a glass rod the graphene oxide was spread evenly over ca. 1 cm^2 of the PET surface. After drying of the graphene oxide deposit, the PET film was removed from the agarose gel and stored under dry conditions. For electrochemical measurements the film was mounted in a U-cell (Figure 1A) between the two glass flanges with the help of some Dow-Corning vacuum grease as sealant.

3. Theory

Ionic diode phenomena in electrolytic systems can often be assigned to more than one mechanism[48] and are dependent on the geometry and materials employed.[42] The crucial part of the ionic diode mechanism treated here is based on diffusion-migration of ions within a cylindrical microhole region in contact to the graphene oxide at one end and in contact to bulk electrolyte solution at the other end (see Figure 2A). The microhole is located as a cylindrical space between a semi-permeable ion-exchange membrane (graphene oxide) and a hypothetical dividing surface indicating the interface to the bulk electrolyte (see area *S* in Figure 2A). The theoretical model is developed here for the case of a cation (or proton) exchange membrane, which during current flow affects concentration gradients of both the cation and the anion in the microhole region (whilst maintaining electroneutrality). A voltage is applied to the two solution compartments (here indicated as a simplified two-electrode system). As current flows driven by potential, the electrolyte concentration within the microhole region changes. In other words, the charge is carried with mobile ions outside of the microhole depending on the direction of the current; the mobile ion being the cation within the membrane in the left direction (Figure 2A), and being in the bulk electrolyte in the right direction. The current is controlled by an electric resistance within the microhole, which is variable and dependent on the applied voltage. This switching of resistivity

with applied potential is observed as “open” and “closed” states of the ionic diode or ionic rectifier.

All relevant variables are defined in Table 1. It is assumed that (i) motion of ions in the microhole is controlled both by diffusion and electric migration; (ii) the Laplace equation for the potential in the solution holds instead of Poisson's equation; (iii) the ionic motion is maintained under steady state; (iv) values for the diffusion coefficients for the electrolyte cation and anion are assumed to be the same; and (v) concentrations of the cation and the anion in the outside solution ($x < 0$) and the membrane ($x > L$) are kept uniformly constant. These assumptions will be examined later. The Laplace equation in the x-direction is given by

$$d^2\phi/dx^2 = 0 \tag{1}$$

to which the boundary conditions, $\phi_{x=0} = 0$ and $\phi_{x=L} = \phi_L$, are applied. The solution is given by a linear potential profile

$$\phi = \phi_L(x/L) \tag{2}$$

The usage of the Laplace equation is based on the equal concentration of the cation and the anion (*i.e.* electroneutrality is maintained). We analyze here the flux and the concentration of only the cation. Since the transport of the ion is controlled by diffusion and electric migration, the flux is represented by

$$f(x) = - D dc/dx - (DF/RT)c\,(d\phi/dx) \tag{3}$$

The equation of continuity, that is, no sink or no source of the cation, is represented by $df/dx = 0$. Therefore, the flux f is a constant. Then Eq. 3 is reduced to

$$dc/dx = -(u/L)(c + Lf/Du) \quad (4)$$

where $u = F\phi_L/RT$. A solution with the condition $c_{x=0} = c_s$ is

$$c = -Lf/Du + (c_s + Lf/Du)\, e^{-ux/L} \quad (5)$$

Applying the condition of $c_{x=L} = c_m$ yields the expression for the flux

$$f = (Du/L)(c_m - c_s e^{-u})/(e^{-u} - 1) \quad (6)$$

The observed current, $I = -AFf$, is given by

$$I = (AF^2 D\phi_L/LRT)(c_m - c_s e^{-u})/(1 - e^{-u}) \quad (7)$$

When $|u|$ is an extremely large value, Eq. 7 for $u > 0$ tends to

$$I = (AF^2 D/LRT) c_m \phi_L \quad (8)$$

while that for $u < 0$ does to

$$I = (AF^2 D/LRT) c_s \phi_L \quad (9)$$

Both expressions for the current at high overpotential represent a linear (Ohmic) characteristic in the variation of I with ϕ_L, although a point of undefined current remains at $u = 0$. The comparison of Eq. 8 and 9 suggests the asymmetric current-voltage curves. By taking the ratio of Eq. 8 to 9, the rectification ratio is estimated as c_m/c_s, which is the concentration ratio of the mobile ion in the ion-exchange membrane ion to that in

the bulk. A plot of the current versus potential based on equation 7 is shown in Figure 2B. Here, c_s = 10 mM has been selected with $D = 10^{-9}$ m^2s^{-1} and $A = \pi r^2$ with a microhole radius r = 10 μm. The apparent membrane concentration c_m = 0.2 M is selected to approximately represent the conditions in experimental data (*vide infra*). Note that the currents are predicted to scale linearly with microhole area A or with r^2 with all other parameters remaining. The rectification ratio is predicted to be independent of microhole diameter.

Since the applied voltage necessarily includes an additional voltage loss from the solution and the membrane as well as further access diffusional losses, the equations given above have to be considered only as a first approximation. The voltage drop is given by $V = I\ (R_{microhole} + R_{additional})$, where $R_{microhole}$ is the resistance ϕ_L/I as given in Eq. 7. So far as difference in the slope is concerned, in the linear domain, Eq. 8 and 9 are valid. In other words, diffusion-only processes can contribute only to the restricted potential domain of $|V| < 0.1$ V. By combining Eq. 5 and 6, concentration profiles within the microhole are expressed by

$$c/c_s = [(c_m/c_s)(1-e^{-xu/L}) + e^{-xu/L} - e^{-u}]/(1 - e^{-u}) \qquad (10)$$

Calculated concentration profiles are plotted against x/L in Figure 2C for four values of ϕ_L. When electric migration does not contribute to the current, the profile is a line (ϕ_L = 0, not shown), as is obvious for conventional steady-state diffusion. With an increase in the contribution of the electric field by positive voltage, the cations and anions move largely toward x = 0, exhibiting concave curves and causing accumulation of salt into the microhole. The application of the opposite voltage causes a depletion of salt in the microhole (Figure 2C). Note that currents in Figure 2B should scale with the square of microhole radius.

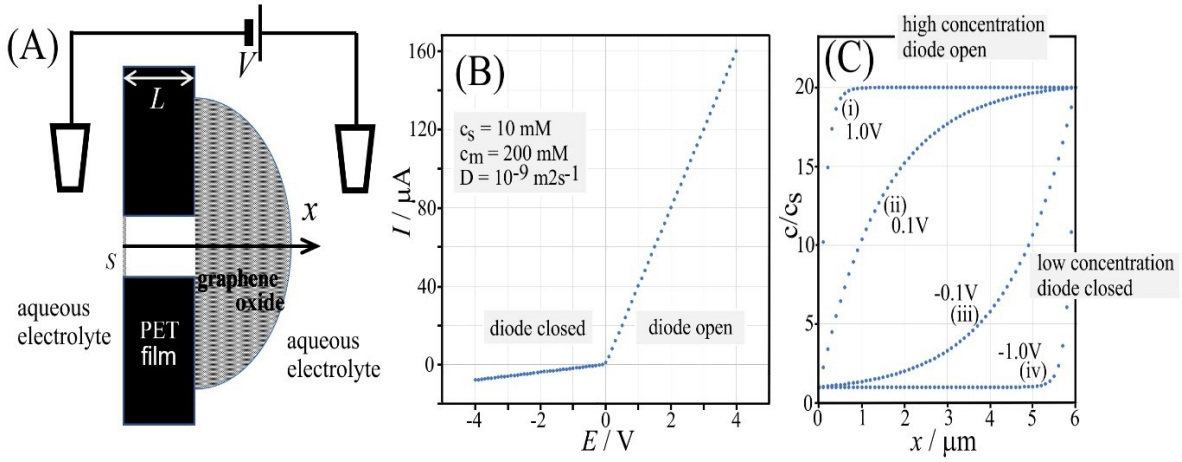

Figure 2. (A) Description of the cylindrical geometry based on surface S and length x within the microhole. Note that the working electrode is always placed on the side of the graphene oxide deposit and therefore a positive applied potential is associated with cation moving from the right into the left compartment. (B) Plot of calculated current from Eq. 7 versus applied potential for the case c_m = 200 mM and c_s = 10 mM. (C) Plot of concentration profiles calculated from Eq (10) at ϕ_L = 1.0 V, 0.1 V, -0.1 V -1.0 V for L = 6 µm.

There are some limitations to quantitative insights due to simplifications made in the present model: (A) If the microhole is so narrow that electric migration force varies with the distance normal to x-direction (e.g. in nanopores), it is necessary to take into account the surface effects such as zeta potential. This subject is beyond the present work. (B) The model does not include mass transport or polarization in the two outer domains of the microhole ($x < 0$ and $x > L$). Diffusion in the outer domains will have to be taken into account due to access diffusion effects. That is, the assumption that c_s = constant at $x = 0$ is not strictly valid and in reality the depletion of salt in the microhole will progress well below $c/c_s = 1$ (see Figure 2C), if the applied potential is sufficiently negative. (C) The assumption of the Laplace equation validity rather than the Poisson's equation validity is based on the equi-concentrations of the anion and the cation (electroneutrality), which is fulfilled at micrometer scale. The Debye length in 10 mM aqueous solution is only ca. 4 nm. This length is too short to consider a domain of x for the difference in concentrations. Therefore, the Laplace equation is valid. We can

compare Eq. 7 with some experimental results obtained for example with Nafion films deposited onto a microhole in PET:[45]

(i) The *I-V* curve in Figure 2B is close in shape to experimental data, in that there are basically composed of two lines with different slopes at positive and negative potentials. The line is consistent with control by electric migration in the microhole region.

(ii) The theoretical rectification ratio is given approximately by c_m/c_s, which predicts the proportionality of the ratio to $1/c_s$. The experimental results, however, are inconsistent with the proportionality. Both, a constant c_m and a constant c_s are likely to be oversimplifications in the model that lead to these inconsistencies.

(iii) According to the present theory, the rectification ratio should be independent of hole diameters. However, the experimental results show some variation in the rectification ratio with the increase in the microhole diameters for (5, 10, 20 μm). Since the thickness of the film remains at 6 μm, the rectification ratio may be affected to some extent by conditions outside of the microhole (*vide infra*).

Further comparison of theory and data obtained for graphene oxide (*vide infra*) shows that equations 7 and 10 are beneficial mainly at qualitative level due to some oversimplifications, but the description of the underlying rectification mechanism and the conditions within the microhole region are very useful to rationalize and predict the observed ionic diode effects.

Table 1. Nomenclature

A	area of the cross-section of the microhole
c	concentration of the cation in the microhole
c_m	concentration of the cation in the adjacent cationic exchange membrane

c_s concentration of the cation in the adjacent solution bulk

D diffusion coefficient of the cation or anion

f flux of the cation in the x-direction

F Faraday constant

I total current

L thickness of the film through which the microhole is made

R gas constant

R_h resistance in the hole, defined by ϕ_L/I

T absolute temperature

u dimensionless potential, $\phi_L F/RT$

x axis along the hole

V voltage between the two cells

ϕ electric potential in the solution

ϕ_L electric potential at $x = L$

4. Results and Discussion

4.1. Formation and Characterization of Graphene Oxide Based Ionic Diodes

Graphene oxide material dispersed in aqueous solution (commercial) consists of single and few-layer nanosheets with typically 2-10 μm size as shown in the transmission electron micrograph in Figure 3A. The deposition of these graphene oxide nanosheets from colloidal suspension onto a PET substrate with 20 μm diameter microhole is performed on an agarose gel substrate[45] to achieve asymmetric deposition and to avoid penetration of the graphene oxide into and below the microhole. When depositing a graphene oxide film together with small amounts of rhodamine B dye, a fluorescent film is produced in order to better visualize the film deposit. The fluorescence microscopy image stack shown in Figure 3B shows the microhole in the x-y plane. Due to light refraction effects, the microhole region appears bright (see white region in

Figure 3B) and also the fluorescence in this region is enhanced (see red region in Figure 3B). In the cross-sectional data the continuous graphene oxide film coated over the microhole can be seen (with an estimated ca. 9-12 μm thickness).

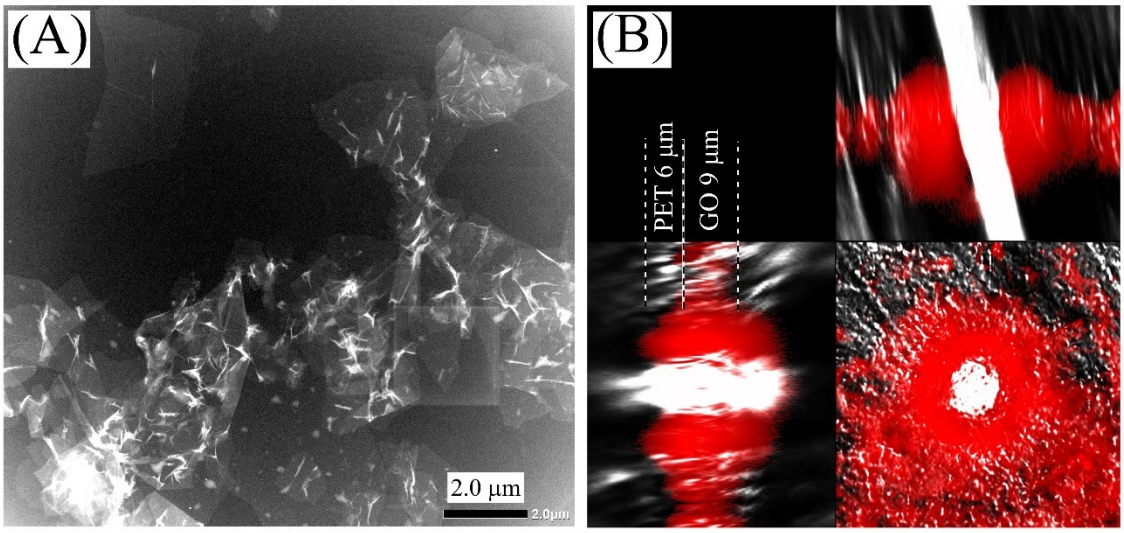

Figure 3. (A) Scanning transition electron microscopy (STEM) image showing graphene oxide flakes of typically 2 to 10 μm size. (B) Fluorescence microscopy image stack for a graphene oxide film with rhodamine B dye. The microhole is clearly seen and the thickness of the graphene oxide (GO) layer is estimated as 9-12 μm.

4.2. Electrochemical Characterization of Graphene Oxide Based Ionic Diodes

When scanning the external potential applied to the graphene oxide deposit (always situated on the side of the working electrode compartment; see Figure 1A), a current response is measured (see Figure 4A). This current response is highly reproducible and insensitive for example to doubling the amount of graphene oxide deposit. This observation is consistent with the simplified theoretical idea of electrolyte accumulation/depletion within the microhole dominating the diode character rather than the potential drop across the graphene oxide deposit. With aqueous 10 mM HCl in both compartments, the current rises with positive applied potential and only a much lower current response is observed with a negative potential applied to the film. Both

branches of the voltammogram appear linear and consistent with the theory (see plot in Figure 2B). This behavior can be described as rectification or ionic diode characteristic. Comparison with theory suggests for c_s = 10 mM the apparent concentration in the graphene oxide should be c_m = 200 mM with a corresponding rectification ratio of 20. Although the match in voltammogram shape between theory and experiment is impressive, one has to be careful with oversimplifying assumptions in the theory. Additional effects do arise (*vide infra*) at both the graphene oxide – electrolyte interface and the access diffusion region close to surface *S* (Figure 2A). Three consecutive potential cycles (scan rate 50 mVs^{-1}) suggest almost time independent (steady state) behavior. When increasing the scan rate to 500 mVs^{-1} (Figure 4B) a slight loop in the current at positive applied potential shows that the current increases with time. At an even faster scan rate (4000 mVs^{-1}, Figure 4C) each consecutive potential scan shows an increase in current. Therefore, the steady state character is lost at a time scale of typically 1 s. In this high scan rate case, also a small peak of negative current appears at -0.3 V indicative of a "switching" process in the diode (between open and closed state) taking approximately 0.2 s. Based on the assumption of a diffusion-migration mechanism, this switching time is likely to be associated with the diffusion of cations and anions to and from the microhole region. This is confirmed by changes in switching time data for different microhole diameters (*vide infra*). However, possibly related "hysteresis" effects on a similar time scale have also been reported for nano-fluidic diodes based on nanopipettes of typically 60 nm orifice diameter[49,50] and attributed to time-dependent compositional changes within the nanopore double layer. This kind of compositional change could also occur within the graphene oxide film and then lead to phenomena like those observed in Figure 4C. This as well as the development of significant concentration gradients within the graphene oxide are clearly possible, but currently not readily accessible by experiment.

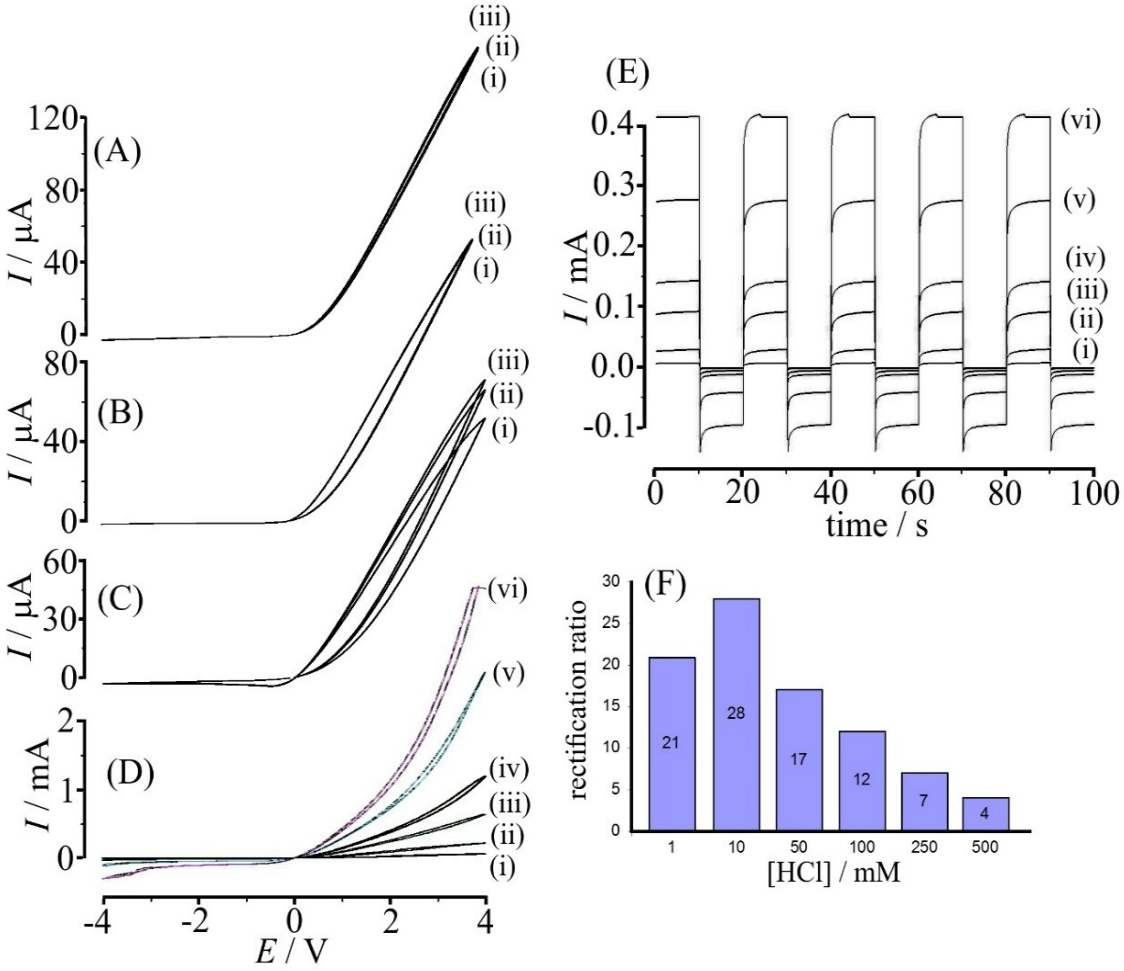

Figure 4. (A) Cyclic voltammograms (scan rate 50 mVs^{-1}; three potential cycles indicated as (i), (ii), and (iii)) for a graphene oxide deposit on a 20 μm diameter microhole in a PET substrate immersed in 10 mM aqueous HCl. (B) As above, scan rate 500 mVs^{-1}. (C) As above, scan rate 4000 mVs^{-1}. (D) As above, scan rate 50 mVs^{-1} for a HCl concentration of (i) 1, (ii) 10, (iii) 50, (iv) 100, (v) 250, (vi) 500 mM. (E) Chronoamperometry data stepping from +1 V to -1V. (F) Plot of the rectification ratio (the absolute of the current at +1 V divided by the current at -1 V) *versus* concentration.

The effect of the HCl concentration on the ionic rectifier response is shown in Figure 4D. In previous reports on ionic diode phenomena higher electrolyte concentration always caused detrimental effects (loss of rectification ability) on the ionic diode behaviour, but (perhaps surprisingly) for graphene oxide even at 0.5 M HCl the

rectification effect is maintained (at least in part). This behaviour for graphene oxide is of interest and important, for example with desalination applications in mind (*vide infra*).[51] When working with aqueous HCl concentrations of 0.1 M and higher, new phenomena occur at applied potentials higher than +3 V and lower than -3 V. In both cases currents increase (non-linearly), which may be caused by "over-limiting" conditions associated with additional convection driven transport.[52] Generally, the characteristics observed in *I-V* curves under steady state conditions (at not too high potentials) are at qualitative level consistent with that predicted in Eq. 7.

Chronoamperometry data are presented in Figure 4E to indicate the switching speed of the diode. For both, positive and negative applied potentials, it appears to take approximately 10-20 s for steady state to be fully reached, but most of the switching occurs within 1 s. Figure 4F shows a plot of the rectification ratio (based on chronoamperometry data) *versus* HCl concentration and a decline at higher concentration is clearly observed. This effect could be associated with the behaviour of the graphene oxide membrane and gradual loss of semi-permeability (which was assumed to be maintained in the theoretical model).

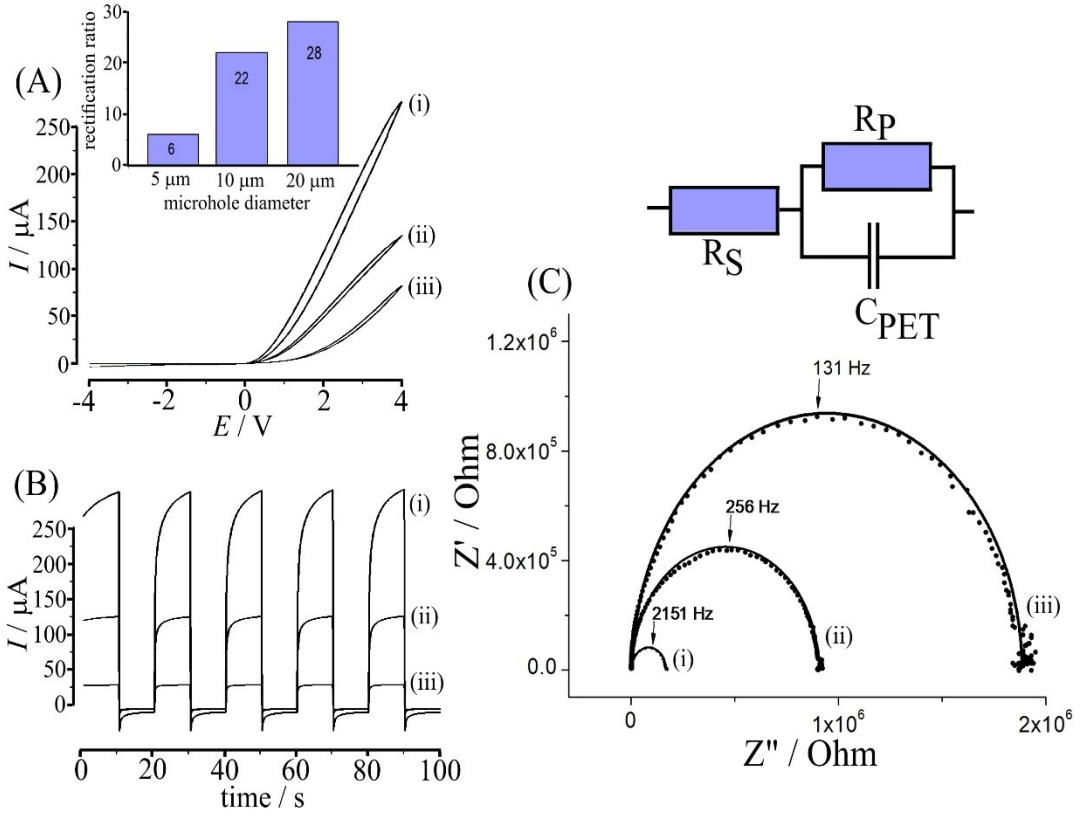

Figure 5. (A) Cyclic voltammograms (scan rate 50 mVs^{-1}) for a graphene oxide deposit on a (i) 20 (ii) 10, (iii) 5 µm diameter microhole in a PET substrate immersed in 10 mM aqueous HCl. Inset: Plot of the rectification ratio (the absolute of the ratio of currents at +1 V and at -1 V) *versus* microhole diameter. (B) Chronoamperometry data stepping from +1 V to -1V. (C) Impedance data (frequency range 50 kHz to 0.5 Hz, amplitude 100 mV, bias 0.0 V; for (i) 20, (ii) 10, and (iii) 5 µm diameter microhole) showing experimental data points and a line for fitting results.

It is interesting to expand the experimental study to the case of different microhole diameters. Figure 5A shows data from cyclic voltammetry experiments performed in aqueous 10 mM HCl for microhole diameters of (i) 20, (ii) 10, and (iii) 5 µm. Currents do scale with microhole diameter in approximately linear manner, but not quadratic as predicted by the theory. Therefore, for a more quantitative description, access diffusion towards the microhole in particular for smaller diameter microholes cannot be

completely ignored. Also, a change in time constant is observed with small diameter microhole devices switching substantially faster (see chronoamperometry data in Figure 5B), which is linked to both access diffusion and diffusion inside of the cylindrical region in the microhole. Diffusion-migration times within the microhole are only dependent on the length *L* and therefore unlikely to change with microhole diameter. External or access diffusion (dependent on *r*) is affected and therefore can explain the decrease in switching time for slower microhole diodes. An approximate expression for the approach of a transient to within 2% of steady state diffusion at microelectrodes has been proposed by Oldham and Myland[53] (see equation 11).

$$\text{time to 2\% within steady state} = 2500 \ \frac{r^2}{\pi D} \qquad (11)$$

In this expression *r* is the microhole radius and *D* is the diffusion coefficient assumed here to be approximately 10^{-9} m^2s^{-1}. For a microhole diameter of 5, 10, and 20 μm, this suggests a time to steady state of approximately 5s, 20 s, and 80 s, respectively, consistent with data in Figure 5B. Additional impedance data have been obtained at 0.0 V (see Figure 5C) as well as at -1.0 V and at +1.0V (see Table 2). These data also confirm that a change in electrolyte concentration occurs locally in the vicinity of the microhole during ionic diode switching.

Table 2. Summary of impedance data obtained in aqueous 10 mM HCl (frequency range 50 kHz to 0.5 Hz, amplitude 100 mV, bias -1.0 V, 0.0 V, or +1.0 V; for 20, 10, and 5 μm diameter microhole; only the high frequency semicircular part of the data are analysed).

microhole diameter	**Rs / Ω**	**Rp / kΩ**	**C_{PET} / nF**
bias 0.0 V			
20 μm	2273 ± 10	166.8 ± 12	0.54 ± 0.001
10 μm	5921 ± 22	900 ± 28	0.55 ± 0.001
5 μm	8320 ± 42	1876 ± 58	0.67 ± 0.001
bias +1.0 V (open diode)			
20 μm	1260 ± 3	32.2 ± 3.5	0.53 ± 0.001
10 μm	1562 ± 7	161.9 ± 8.6	0.52 ± 0.001
5 μm	6467 ± 27	800 ± 40	0.32 ± 0.001
bias -1.0 V (closed diode)			
20 μm	9992 ± 97	192.6 ± 0.26	0.56 ± 0.001
10 μm	14620 ± 200	2900 ± 4.3	0.52 ± 0.001
5 μm	17870 ± 280	13880 ± 10	0.35 ± 0.001

The capacitance C_{PET} of the PET film remains constant under all conditions. The resistance R_S (dominated by the solution phase in the vicinity of the microhole) shows an increase with smaller microhole diameter. The R_P resistance linked with PET film polarization (associated with both graphene oxide resistivity and electrolyte resistivity within the microhole region) also increases for smaller microhole diameters. Crucially, both R_S and R_P change when switching the diode from open (+1.0 V) to closed state (-1.0 V). This suggests that the electrolyte solution plays a significant role. Additional effects arising form charge carrier concentration gradients within the graphene oxide and from the graphene oxide|electrolyte interface are also likely (*vide infra*).

Finally, the rectification ratio when investigated as a function of microhole diameter (see inset in Figure 5A) shows a downward variation for smaller diameter microholes. This behavior is outside of the simplified theory (which predicts a constant rectification ratio) and associated with the diffusion-migration behavior external to the microhole region or within the graphene oxide. The proposed simplified theoretical model provides a good model system to explain ionic rectifier effects based on the electrolyte-based processes within the microhole region. However, processes within the graphene oxide cannot be ignored and more work will be needed in future to refine the theory and better (more quantitatively) predict characteristics such as rectification ratio and switching time for these ionic diode systems.

4.3. Na^+ versus H^+ Selectivity at Graphene Oxide Based Ionic Diodes

Next, the graphene oxide based ionic diode is investigated in aqueous NaOH and in aqueous NaCl. In previous studies, for example based on cellulose materials,[46] the type of electrolyte and the pH of the solution were important parameters affecting the behavior of the ionic diode. Data for the graphene oxide diode in aqueous NaOH is shown in Figure 6A. Rectification effects very similar to those in Figure 4A for aqueous HCl are observed and the shape of the diode response could be consistent with that of a cationic diode (open in the positive potential range). Chronoamperometry data are shown in Figure 6B and rectification ratio data are summarized in Figure 6C. Rectification effects are substantial and almost independent of ionic strength, but generally lower than those observed in the presence of aqueous HCl.

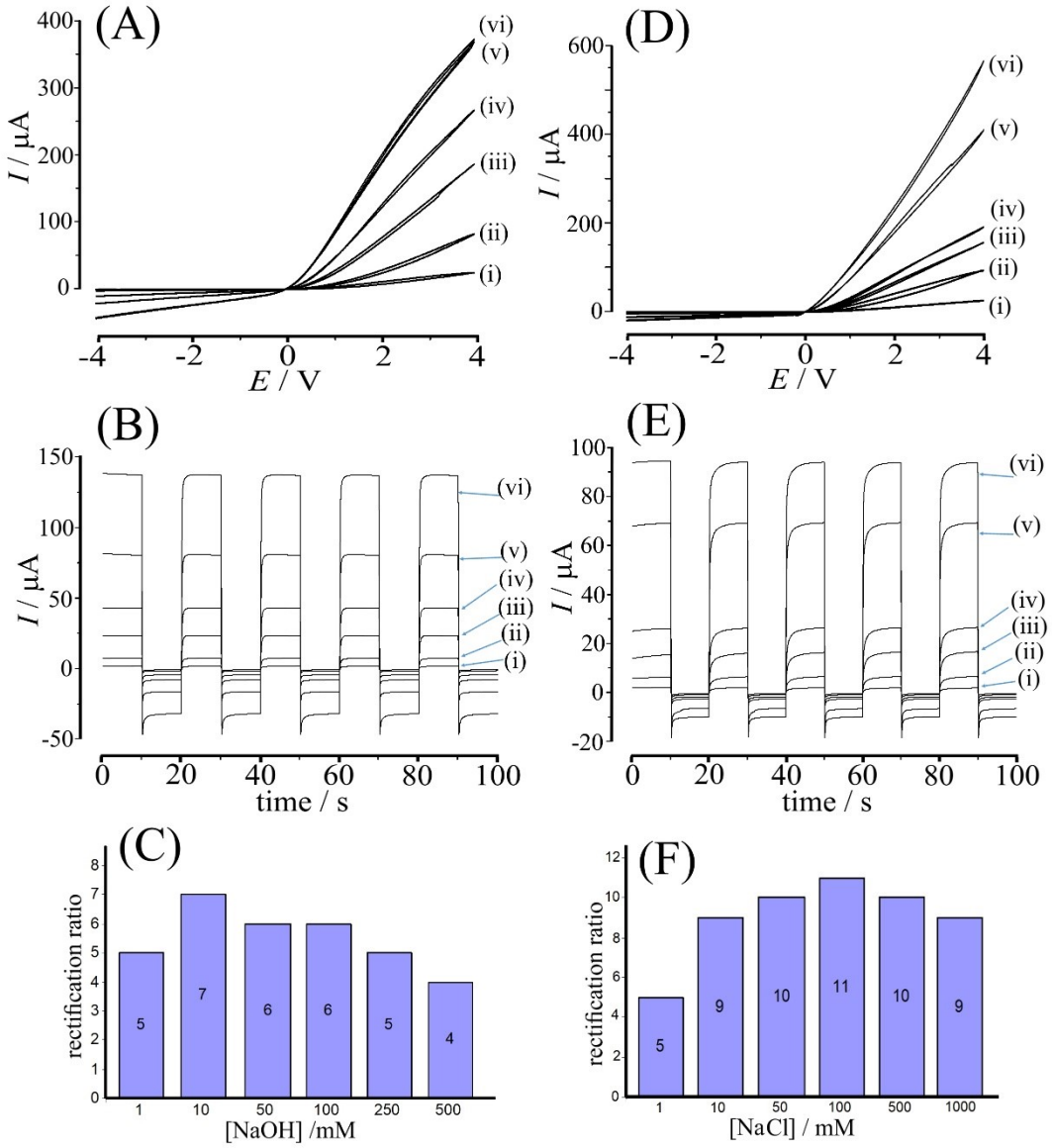

Figure 6. (A) Cyclic voltammograms (scan rate 50 mVs^{-1}) for a graphene oxide deposit on a 20 µm diameter microhole in a PET substrate immersed in (i) 1, (ii) 10, (iii) 50, (iv) 100, (v) 250, and (vi) 500 mM aqueous NaOH. (B) Chronoamperometry data stepping from +1 V to -1V. (C) Plot of the rectification ratio (the absolute of the current at +1 V divided by the current at -1 V) *versus* NaOH concentration. (D) Cyclic voltammograms (scan rate 50 mVs^{-1}) for a graphene oxide deposit on a 20 µm diameter microhole in a PET substrate immersed in (i) 1, (ii) 10, (iii) 50, (iv) 100, (v) 500, and (vi) 1000 mM aqueous NaCl. (E) Chronoamperometry data stepping from +1 V to -1V. (F) Plot of the rectification ratio (the absolute of the current at +1 V divided by the current at -1 V) *versus* NaCl concentration.

Next, in Figure 6D data are shown for aqueous NaCl in a concentration range from 1 mM to 1000 mM. Cyclic voltammetry and chronoamperometry data suggest a substantial rectification effect again observed over the complete concentration range and most effective in the 100 mM range (see Figure 6F). These results are promising in view of future desalination applications, but also unusual (when compared to ionic diodes based on other types of semipermeable ionomer materials, where higher ionic strength strongly inhibited the rectification effect[45]). A comparison of ionic diode data for 10 mM NaCl, 10 mM NaOH, and 10 mM HCl is shown in Figure 7B. In can be observed that both open diode currents and rectification ratio data are higher for aqueous HCl and essentially identical for NaOH and NaCl. This is likely to be linked to the cation mobility for protons and for Na^+ in graphene oxide dominating the resistance for the open diode. The mobility at 298 K[54] for H^+ in aqueous media (36.23×10^{-8} $m^2V^{-1}s^{-1}$) and for Na^+ in aqueous media (5.19×10^{-8} $m^2V^{-1}s^{-1}$) suggests substantially higher mobility for protons, but here this is likely to be moderated by host interactions within the graphene oxide.

The question of cation selectivity in transport across the graphene oxide film requires further experimental insight to reveal the nature of the ion responsible for the current response. It is possible that proton transport could dominate even in electrolyte media based on Na^+ cations. Field driven heterolytic water dissociation has recently been proven to occur for example at Fumasep ionomer ionic diodes[55] under similar conditions. The localized formation of H^+ and OH^- associated with this heterolytic water dissociation is known to occur as a potential-driven catalytic process at membrane surfaces, for example when catalyzed by graphene oxide derivatives[56] or nanosheet MoS_2.[57] This type of competing process should lead to measurable pH gradients between right compartment and left compartment. Therefore, additional experiments are performed here with pH probes independently monitoring the local pH

in the right and in the left solution compartments close to the membrane and *in situ* during ionic diode operation. Figure 7A shows a schematic drawing of the experiment. During operation of the "open diode" in aqueous 10 mM NaCl either transport of (i) Na^+ or transport of (ii) H^+ are plausible. This should result in either (i) no pH change or (ii) a change to higher pH (more alkaline) on the right and lower pH (more acidic) on the left, respectively.

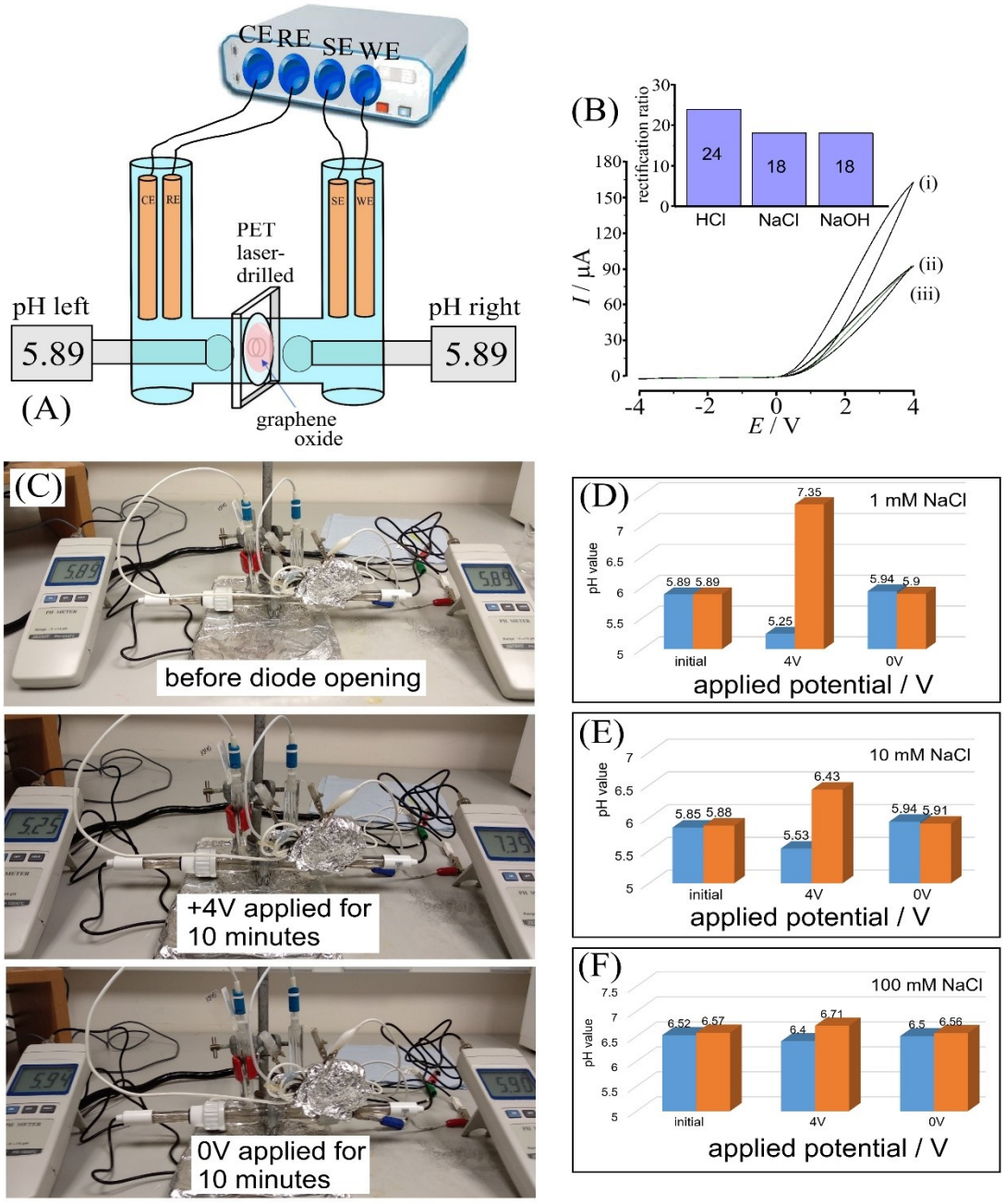

Figure 7. (A) Schematic drawing of the 4-electrode measurement cell fitted with two additional pH meters. (B) Cyclic voltammograms (scan rate 50 mVs^{-1}) for a graphene oxide deposit on a 20 µm diameter microhole in a PET substrate immersed in 10 mM (i) HCl, (ii) NaCl, and (iii) NaOH. (C) Photographs showing the measurement cell with 1 mM NaCl before diode opening, after 10 minutes +4V open diode operation, and after further 10 minutes 0V closed diode operation. Also shown are bar plots for pH changes observed under these conditions for (D) 1 mM NaCl, (E) 10 mM NaCl, and (F) 100 mM NaCl.

It is possible to express the approximate effect of a proton current through the diode in terms of the pH in the right and in the left compartment when assuming a fixed volume V of ca. 0.01 dm^3 (an estimated volume where pH changes occur close to the membrane surface) to be relevant right and left of the membrane. Equations 12 and 13 express the shift in pH (from an initial value pHi) in the right compartment (where protons are lost) in the left compartment (where protons are gained). Other parameters are the time-average absolute current I, the time t = 600 s, and the Faraday constant F = 96487 C mol^{-1}.

$$pH_{left} = -\log_{10}(10^{-pHi} + It/FV) \quad (12)$$

$$pH_{right} = 14 + \log_{10}(10^{-(14-pHi)} + It/FV) \quad (13)$$

For the case of a 1 mM NaCl electrolyte (see Figure 7D) the average current at an applied voltage of 4 V was 17 μA over 600 s, which (with pHi = 5.89) translates to pH_{left} = 4.9 and pH_{right} = 9.0. Comparison to the experimental results in Figure 7D shows that the predicted trend is indeed observed, but it shows also that the effect is less strong. This suggests that a competition of Na^+ transport and H^+ transport occurs. When increasing the concentration to 10 mM NaCl (Figure 7E) the observed current was 45 μA at 4 V applied voltage. According to equations 12 and 13 the predicted values are pH_{left} = 4.5 and pH_{right} = 9.4. The increase in NaCl concentration therefore lowers the rate of production of protons and hydroxide. Finally, with 100 mM NaCl electrolyte the observed average current was 112 μA at 4 V applied voltage, which suggests pH_{left} = 4.1 and pH_{right} = 9.8. The observed values of pH_{left} = 6.4 and pH_{right} = 6.7 (Figure 7F) suggest a minimal contribution from water heterolysis under these conditions. Therefore, graphene oxide offers a material able to rectify Na^+ cation currents with good efficiency and at relatively high ionic strength (consistent with that

of seawater). It has recently been reported that the ionic diode effect can be developed into an ionic current rectifier for desalination[51] based on AC excitation from capacitive driver electrodes. Ideal for this purpose would be a device combining a Na^+ ionic rectifier (cationic diode) and a Cl^- ionic rectifier (anionic diode) to transfer both cations and anions uni-directionally and irreversibly across a membrane. With sufficient rectification ratio, this will transfer salt and lower the concentration level in one of the two compartments (for example removing 90% of salt). In order to achieve this type of process in future, it will be necessary to identify a complementary anionic diode material similarly effective as the graphene oxide cationic diode material, but selective for chloride anions.

5. Conclusions

In summary, it has been shown that graphene oxide can be readily deposited onto a microhole in PET to give a novel ionic current rectifier (or cationic diode) device. Proton transport through the graphene oxide is facile and therefore accumulation and depletion effects in the microhole region are suggested to be mainly responsible for the diode effects. The diode effect persists even at higher concentrations of hydrochloric acid, which can be ascribed to porosity effects in the graphene oxide and sustained semi-permeability. Very similar behavior was observed in electrolyte media containing NaOH and NaCl and it has been shown that Na^+ ionic currents are dominant even down to relatively low concentrations of Na^+ (with minimal competition due to proton transport). The system appears promising (in particular in the context of desalination applications), but has to be investigated in more detail and for a wider range of aqueous electrolyte systems. The effects of graphene oxide structure and chemically modified graphene oxides need to be explored. The co-transport of small molecule species (e.g. H_2O) during ionic diode operation is likely to result in AC-driven “molecular pump” effects and this also needs further attention.

To develop a more quantitative theoretical description and better insight into the various aspects of the diode mechanism, the simplified theoretical model developed here (based only on phenomena in the electrolytes solution within the microhole region) could be refined by including phenomena within the graphene oxide and within the access diffusion region. Alternatively, computational simulation tools could be employed to add in complexity due to diffusivity of cations and anions, due to charge carrier mobility and concentration gradients within the graphene oxide, or due to interfacial phenomena at the ionomer – electrolyte interface. In this study, the underlying mechanistic foundation based on the salt depletion and salt accumulation phenomena in the microhole region are clearly demonstrated. The methodology employed here will allow screening of a wider range of materials and discovery of suitable anionic diodes to complement the behavior of graphene oxide as cationic diode in desalination.

Acknowledgements

B.R.P. thanks to Indonesian Endowment (LPDP RI) for a PhD scholarship.

References

(1) Loh, K.P.; Bao, Q.L.; Eda, G.; Chhowalla, M. Graphene Oxide as a Chemically Tunable Platform for Optical Applications. *Nature Chem.* **2010**, *2*, 1015–1024.

(2) Surwade, S.P.; Smirnov, S.N.; Vlassiouk, I.V.; Unocic, R.R.; Veith, G.M.; Dai, S.; Mahurin, S.M. Water Desalination Using Nanoporous Single-layer Graphene. *Nature Nanotechnol*. **2015**, *10*, 459–464.

(3) Han, Y.; Xu, Z.; Gao, C. Ultrathin Graphene Nanofiltration Membrane for Water Purification. *Adv. Functional Mater.* **2013**, *23*, 3693–3700.

(4) Choi, B.G.; Hong, J.; Park, Y.C.; Jung, D.H.; Hong, W.H.; Hammond, P.T.; Park, H. Innovative Polymer Nanocomposite Electrolytes: Nanoscale Manipulation of Ion Channels by Functionalized Graphenes. *ACS Nano* **2011**, *5*, 5167–5174.

(5) Joshi, R.K.; Carbone, P.; Wang, F.C.; Kravets, V.G.; Su, Y.; Grigorieva, I.V.; Wu, H.A.; Geim, A.K.; Nair, R.R. Precise and Ultrafast Molecular Sieving Through Graphene Oxide Membranes. *Science* **2014**, *343*, 752–754.

(6) Sun, P.Z.; Zhu, M.; Wang, K.L.; Zhong, M.L.; Wei, J.Q.; Wu, D.H.; Xu, Z.P.; Zhu, H.W. Selective Ion Penetration of Graphene Oxide Membranes. *ACS Nano* **2013**, *7*, 428–437.

(7) Nair, R.R.; Wu, H.A.; Jayaram, P.N.; Grigorieva, I.V.; Geim, A.K. Unimpeded Permeation of Water Through Helium-Leak-Tight Graphene-Based Membranes. *Science* **2012**, *335*, 442–444.

(8) Huang, H.B.; Song, Z.G.; Wei, N.; Shi, L.; Mao, Y.Y.; Ying, Y.L.; Sun, L.W.; Xu, Z.P.; Peng, X.S. Ultrafast Viscous Water Flow Through Nanostrand-Channeled Graphene Oxide Membranes. *Nature Commun.* **2013**, *4*, 2979.

(9) Huang, H.B.; Mao, Y.Y.; Ying, Y.L.; Liu, Y.; Sun, L.W.; Peng, X.S. Salt Concentration, pH and Pressure Controlled Separation of Small Molecules Through Lamellar Graphene Oxide Membranes. *Chem. Commun.* **2013**, *49*, 5963–5965.

(10) Karim, M.R.; Islam, M.S.; Rabin, N.N.; Takehira, H.; Wakata, K.; Nakamura, M.; Ohtani, R.; Toda, K.; Hayami, S. Interlayer Void Space as the Key Semipermeable Site for Sieving Molecules and Leaking Ions in Graphene Oxide Filter. *ChemistrySel*. **2017**, *2*, 4248–4254.

(11) Zhang, Y.; Zhang, S.; Chung, T.S. Nanometric Graphene Oxide Framework Membranes with Enhanced Heavy Metal Removal via Nanofiltration. *Environm. Sci. Technol.* **2015**, *49*, 10235–10242.

(12) Yeh, C.N.; Raidongia, K.; Shao, J.J.; Yang, Q.H.; Huang, J.X. On the Origin of the Stability of Graphene Oxide Membranes in Water. *Nature Chem.* **2015**, *7*, 166–170.

(13) Abraham, J.; Vasu, K.S.; Williams, C.D.; Gopinadhan, K.; Su, Y.; Cherian, C.T.; Dix, J.; Prestat, E.; Haigh, S.J.; Grigorieva, I.V.; Carbone, P.; Geim, A.K.; Nair, R.R. Tunable Sieving of Ions Using Graphene Oxide Membranes. *Nature Nanotechnol*. **2017**, *12*, 546–549.

(14) Shi, J.L.; Wu, W.F.; Xia, Y.; Li, Z.J.; Li, W.B. Confined Interfacial Polymerization of Polyamide-Graphene Oxide Composite Membranes for Water Desalination. *Desalination* **2018**, *441*, 77–86.

(15) Sun, P.Z.; Zheng, F.; Zhu, M.; Song, Z.G.; Wang, K.L.; Zhong, M.L.; Wu, D.H.; Little, R.B.; Xu, Z.P.; Zhu, H.W. Selective Trans-Membrane Transport of Alkali and Alkaline Earth Cations through Graphene Oxide Membranes Based on Cation-pi Interactions. *ACS Nano* **2014**, *8*, 850–859.

(16) Joshi, R.K.; Alwarappan, S.; Yoshimura, M.; Sahajwalla, V.; Nishina, Y. Graphene Oxide: the new Membrane Material. *Appl. Mater. Today* **2015**, *1*, 1–12.

(17) Eftekhari, A.; Shulga, Y.M.; Baskakov, S.A.; Gutsev, G.L. Graphene Oxide Membranes for Electrochemical Energy Storage and Conversion. *Internat. J. Hydrogen Energy* **2018**, *43*, 2307–2326.

(18) Martinez, J.G.; Otero, T.F.; Bosch-Navarro, C.; Coronado, E.; Marti-Gastaldo, C.; Prima-Garcia, H. Graphene Electrochemical Responses Sense Surroundings. *Electrochim. Acta* **2012**, *81*, 49–57.

(19) Hu, M.; Mi, B.X. Layer-by-layer Assembly of Graphene Oxide Membranes via Electrostatic Interaction. *J. Membrane Sci.* **2014**, *469*, 80–87.

(20) Liu, H.Y.; Wang, H.T.; Zhang, X.W. Facile Fabrication of Freestanding Ultrathin Reduced Graphene Oxide Membranes for Water Purification. *Adv. Mater*. **2015**, *27*, 249–254.

(21) Zhang, S.P.; Li, D.; Kang, J.X.; Ma, G.P.; Liu, Y. Electrospinning Preparation of a Graphene Oxide Nanohybrid Proton-Exchange Membrane for Fuel Cells. *J. Appl. Polym. Sci.* **2018**, *135*, 46443.

(22) Farooqui, U.R.; Ahmad, A.L.; Hamid, N.A. Graphene Oxide: A Promising Membrane Material for Fuel Cells. *Renew. Sustain. Energy Rev.* **2018**, *82*, 714–733.

(23) Karim, M.R.; Hatakeyama, K.; Matsui, T.; Takehira, H.; Taniguchi, T.; Koinuma, M.; Matsumoto, Y.; Akutagawa, T.; Nakamura, T.; Noro, S.; Yamada, T.; Kitagawa, H.; Hayami, S. Graphene Oxide Nanosheet with High Proton Conductivity. *J. Amer. Chem. Soc.* **2013**, *135*, 8097–8100.

(24) Zarrin, H.; Higgins, D.; Jun, Y.; Chen, Z.W.; Fowler, M. Functionalized Graphene Oxide Nanocomposite Membrane for Low Humidity and High

Temperature Proton Exchange Membrane Fuel Cells. *J. Phys. Chem. C* **2011**, *115*, 20774–20781.

(25) Huang, L.; Li, Y.R.; Zhou, Q.Q.; Yuan, W.J.; Shi, G.Q. Graphene Oxide Membranes with Tunable Semipermeability in Organic Solvents. *Adv. Mater.* **2015**, *27*, 3797–3802.

(26) Sun, P.Z.; Wang, K.L.; Zhu, H.W. Recent Developments in Graphene-Based Membranes: Structure, Mass-Transport Mechanism and Potential Applications. *Adv. Mater.* **2016**, *28*, 2287–2310.

(27) Ping, J.F.; Wang, Y.X.; Ying, Y.B.; Wu, J. Application of Electrochemically Reduced Graphene Oxide on Screen-Printed Ion-Selective Electrode. *Anal. Chem.* **2012**, *84*, 3473–3479.

(28) Zhou, K.G.; Vasu, K.S.; Cherian, C.T.; Neek-Amal, M.; Zhang, J.C.; Ghorbanfekr-Kalashami, H.; Huang, K.; Marshall, O.P.; Kravets, V.G.; Abraham, J.; Su, Y.; Grigorenko, A.N.; Pratt, A.; Geim, A.K.; Peeters, F.M.; Novoselov, K.S.; Nair, R.R. Electrically Controlled Water Permeation Through Graphene Oxide Membranes. *Nature* **2018**, *559*, 236–239.

(29) Jana, S.K.; Banerjee, S.; Bayan, S.; Inta, H.R.; Mahalingam, V. Rectification and Amplification of Ionic Current in Planar Graphene/Graphene-Oxide Junctions: An Electrochemical Diode and Transistor. *J. Phys. Chem. C* **2018**, *122*, 11378–11384.

(30) Zhang, Z.; Wen, L.P.; Jiang, L. Bioinspired Smart Asymmetric Nanochannel Membranes. *Chem. Soc. Rev.* **2018**, *47*, 322–356.

(31) Zhu, X.B.; Zhou, Y.H.; Hao, J.R.; Bao, B.; Bian, X.J.; Jiang, X.Y.; Pang, J.H.; Zhang, H.B.; Jiang, Z.H.; Jiang, L. A Charge-Density-Tunable Three/Two-

Dimensional Polymer/Graphene Oxide Heterogeneous Nanoporous Membrane for Ion Transport. *ACS Nano* **2017**, *11*, 10816–10824.

(32) Wang, L.L.; Feng, Y.P.; Zhou, Y.; Jia, M.J.; Wang, G.J.; Guo, W.; Jiang, L. Photo-switchable Two-dimensional Nanofluidic Ionic Diodes. *Chem. Sci.* **2017**, *8*, 4381–4386.

(33) Rong, Y.Y.; Song, Q.L.; Mathwig, K.; Madrid, E.; He, D.P.; Niemann, R.G.; Cameron, P.J.; Dale, S.E.C.; Bending, S.; Carta, M.; Malpass-Evans, R.; McKeown, N.B.; Marken, F. PH-induced Reversal of Ionic Diode Polarity in 300 nm Thin Membranes Based on a Polymer of Intrinsic Microporosity. *Electrochem. Commun.* **2016**, *69*, 41–45.

(34) Tshwenya, L.; Arotiba, O.; Putra, B.R.; Madrid, E.; Mathwig, K.; Marken, F. Cationic Diodes by Hot-pressing of Fumasep FKS-30 Ionomer Film onto a Microhole in Polyethylene Terephthalate (PET). *J. Electroanal. Chem.* **2018**, *815*, 114–122.

(35) Cheng, L.J.; Guo, L.J. Nanofluidic Diodes. *Chem. Soc. Rev.* **2010**, *39*, 923–938.

(36) Siwy, Z.S. Ion-current Rectification in Nanopores and Nanotubes with Broken Symmetry. *Adv. Funct. Mater*. **2006**, *16*, 735–746.

(37) Lan, W.J.; Edwards, M.A.; Luo, L.; Perera, R.T.; Wu, X.J.; Martin, C.R.; White, H.S. Voltage-Rectified Current and Fluid Flow in Conical Nanopores. *Acc. Chem. Res*. **2016**, *49*, 2605–2613.

(38) Choi, E.; Wang, C.; Chang, G.T.; Park, J. High Current Ionic Diode Using Homogeneously Charged Asymmetric Nanochannel Network Membrane. *Nano Lett.* **2016**, *16*, 2189–2197.

(39) Lovrecek, B.; Despic, A.; Bockris, J.O.M. Electrolytic Junctions with Rectifying Properties. *J. Phys. Chem.* **1959**, *63*, 750–751.

(40) Green, Y.; Edri, Y.; Yossifon, G. Asymmetry-induced Electric Current Rectification in Permselective Systems. *Phys. Rev. E* **2015**, *92*, 033018.

(41) Green, Y.; Eshel, R.; Park, S.; Yossifon, G. Interplay between Nanochannel and Microchannel Resistances. *Nano Lett.* **2016**, *16*, 2744–2748.

(42) Mathwig, K.; Aaronson, B.D.B.; Marken, F. Ionic Transport in Microhole Fluidic Diodes Based on Asymmetric Ionomer Film Deposits. *ChemElectroChem* **2018**, *5*, 897–901.

(43) Guo, W.; Tian, Y.; Jiang, L. Asymmetric Ion Transport through Ion-Channel-Mimetic Solid-State Nanopores. *Acc. Chem. Res*. **2013**, *46*, 2834–2846.

(44) He, X.L.; Zhang, K.L.; Li, T.; Jiang, Y.; Yu, P.; Mao, L.Q. Micrometer-Scale Ion Current Rectification at Polyelectrolyte Brush-Modified Micropipets. *J. Am. Chem. Soc*. **2017**, *139*, 1396-1399.

(45) He, D.P.; Madrid, E.; Aaronson, B.D.B.; Fan, L.; Doughty, J.; Mathwig, K.; Bond, A.M.; McKeown, N.B.; Marken, F. A Cationic Diode Based on Asymmetric Nafion Film Deposits. *ACS Appl. Mater. Interfaces* **2017**, *9*, 11272–11278.

(46) Aaronson, B.D.B.; Wigmore, D.; Johns, M.A.; Scott, J.L.; Polikarpov, I.; Marken, F. Cellulose Ionics: Switching Ionic Diode Responses by Surface Charge in Reconstituted Cellulose Films. *Analyst* **2017**, *142*, 3707–3714.

(47) Madrid, E.; Rong, Y.Y.; Carta, M.; McKeown, N.B.; Malpass-Evans, R.; Attard, G.A.; Clarke, T.J.; Taylor, S.H.; Long, Y.T.; Marken, F. Metastable Ionic Diodes

Derived from an Amine-Based Polymer of Intrinsic Microporosity. *Angew. Chem. Inter. Ed.* **2014**, *53*, 10751–10754.

(48) Putra, B.R.; Carta, M.; Malpass-Evans, R.; McKeown, N.B.; Marken, F. Potassium Cation Induced Ionic Diode Blocking for a Polymer of Intrinsic Microporosity | Nafion "Heterojunction" on a Microhole Substrate. *Electrochim. Acta* **2017**, *258*, 807–813.

(49) Li, Y.; Wang, D.C.; Kvetny, M.M.; Brown, W.; Liu, J.; Wang, G. History-Dependent Ion Transport Through Conical Nanopipettes and the Implications in Energy Conversion Dynamics at Nanoscale Interfaces. *Chem. Sci.* **2015**, *6*, 588–595.

(50) Wang, D.C.; Kvetny, M.; Liu, J.; Brown, W.; Li, Y.; Wang, G. Transmembrane Potential across Single Conical Nanopores and Resulting Memristive and Memcapacitive Ion Transport. *J. Am. Chem. Soc.* **2012**, *134*, 3651–3654.

(51) Madrid, E.; Cottis, P.; Rong, Y.Y.; Rogers, A.T.; Stone, J.M.; Malpass-Evans, R.; Carta, M.; McKeown, N.B.; Marken, F. Water Desalination Concept Using an Ionic Rectifier Based on a Polymer of Intrinsic Microporosity (PIM). *J. Mater. Chem. A* **2015**, *3*, 15849–15853.

(52) Chang, H.C.; Yossifon, G.; Demekhin, E.A. Nanoscale Electrokinetics and Microvortices: How Microhydrodynamics Affects Nanofluidic Ion Flux. *Ann. Rev. Fluid Mechanics* **2012**, *44*, 401–426.

(53) K.B. Oldham, J.C. Myland, *Fundamentals of Electrochemical Science*, Academic Press, London,, 1994, p. 278.

(54) Atkins, P.W.; de Paula, J.; Keeler, J. *Physical Chemistry*, 11th ed., Oxford University Press, Oxford, 2018, p. 702.

(55) Tshwenya, L.; Arotiba, O.; Putra, B.R.; Madrid, E.; Mathwig, K.; Marken, F. Cationic Diodes by Hot-pressing of Fumasep FKS-30 Ionomer Film Onto a Microhole in Polyethylene Terephthalate (PET). *J. Electroanal. Chem.* **2018**, *815*, 114–122.

(56) Manohar, M.; Das, A.K.; Shahi, V.K. Efficient Bipolar Membrane with Functionalized Graphene Oxide Interfacial Layer for Water Splitting and Converting Salt into Acid/Base by Electrodialysis. *Industrial Engineer. Chem. Res*. **2018**, *57*, 1129–1136.

(57) Li, J.; Morthensen, S.T.; Zhu, J.Y.; Yuan, S.S.; Wang, J.; Volodine, A.; Lin, J.Y.; Shen, J.N.; Van der Bruggen, B. Exfoliated MoS_2 Nanosheets Loaded on Bipolar Exchange Membranes Interfaces as Advanced Catalysts for Water Dissociation. *Separation Purification Technol.* **2018**, *194*, 416–424.